https://doi.org/10.33271/nvngu/2023-2/064

B. Eller[1,2],
orcid.org/0000-0001-7253-1757,
S. Szalai[1],
orcid.org/0000-0001-6440-1135,
M. Sysyn[3],
orcid.org/0000-0001-6893-0018,
D. Harrach[1],
orcid.org/0000-0003-4819-8506,
J. Liu[4],
orcid.org/0000-0002-4779-7761,
S. Fischer[*1],
orcid.org/0000-0001-7298-9960

1 – Széchenyi István University, Győr, Hungary
2 – University of Pécs, Pécs, Hungary
3 – Institute of Railway Systems and Public Transport, TU Dresden, Dresden, Federal Republic of Germany
4 – Southwest Jiaotong University, Chengdu, the People's Republic of China
* Corresponding author e-mail: fischersz@sze.hu

INNER SHEAR RESISTANCE INCREASING EFFECT OF CONCRETE CANVAS IN BALLASTED RAILWAY TRACKS

Purpose. To prove that the GCCM (geosynthetic cementitious composite mat) – type Concrete Canvas (CC) – is an adequate supplementary layer on the top of the subgrade. As its drainage function is known, this article tries to prove the reinforcement possibility. This layer is relatively thin; nevertheless, it can behave like the geogrids. It is the main path to finding out the opportunity of the interlocking effect and its impact on the railway ballast's inner shear resistance.

Methodology. The laboratory measurements were performed in a multi-level shear box, which allows simulating the multi-level shift of the ballast layer. The tests were planned with and without the CC layer. After shearing, the samples were also tested for load-bearing capacity (E_2; according to the Hungarian Standard) and particle breakage. On the other hand, the contact surface between the lowest part of the ballast and CC was also measured by a sophisticated 3D laser scanner (GOM ATOS) and graphically by AutoCAD software.

Findings. After the results of the laboratory experiments are analyzed, the following parameters are calculated and determined: 1) the reinforcement ratio as the tangent of the inner shear resistance curves in the 5–15 mm horizontal shearing interval as well as the area under graphs by integration in the 0–40 mm interval; 2) the change in load-bearing capacity of the layer-structure with and without CC; 3) the amount of the cement particles; 4) the amount of the broken particles; 5) contact surface between the lowest layer of ballast and CC; 6) flatness of CC sheets after shearing. Based on the results, the Concrete Canvas provides significant reinforcement to the railway ballast.

Originality. Any other type of measurement with Concrete Canvas in a multi-level shear box is unknown. The topic is unique.

Practical value. In the future, these results may provide baseline data to verify the suitability of the Concrete Canvas in the railway sub- or superstructure for various types of transport.

Keywords: *railway, deterioration, concrete canvas, ballasted track, inner shear resistance, interlocking effect, GOM ATOS*

Introduction. Nowadays, railway track maintenance in Hungary is slightly different from that a few decades ago. Many railway lines have been renewed thanks to the European Union's support [1]. It means brand new subgrades, protection layers (in other words, supplementary layers), and superstructures. With these supports also come additional (extra) requirements. One of these is preventive maintenance [2, 3], which means yearly maintenance like leveling and rail grinding. These two cost a lot, while the other lines need the same or more money. If the amount of maintenance does not increase, there will be no money for maintaining the not frequented railway lines used only by a few trains. However, these mentioned railway lines can also have importance, for example, because of the industry. Even though the mentioned rarely used railway lines have lower traffic, the deterioration and failures in the structures can be the same or worse [4, 5]. Ultimately, these costs come from the same pocket, so that preventive maintenance may take resources from the other sections. New technologies are needed that are easy to handle and increase the lifetime of the railway structure, for example, replacing track slab with lateral pushing rail in one maintenance window time [6], increasing the maintenance reliability of railway curves [7], finite element modeling and parametric investigation of a rail damper [8, 9].

The railway projects and the connecting risk analysis are also worth mentioning when investigating railway tracks, lines, or maybe an entire railway network [10].

In the case of reviewing the international literature related to railway and road transport, researchers dealt with related issues of transportation possibilities in foreign countries [11, 12], as well as quarry ballast [13–15]. Proposed by Naumov, et al. [11], the approach is based on the fuzzy-logic mathematical apparatus and uses the surveys' data to calculate the membership functions. Saukenova, Oliskevych, et al. [12] dealt with the simulation possibilities of cargo delivery by road carrier. Milosevic, et al. [13] investigated the model-based remote health monitoring of ballast conditions in highway-railway grade crossing panels taking into consideration multibody simulation. In this research, the complex wheel-rail interaction in the crossing transition area was considered, using a finite element (FE) representation.

Rao, et al. [16] applied FE simulation based on structural dynamics on a railway freight wagon. The papers [11–13] can be connected to the logistics of ballast: simulation, cost optimization, lowering in transport routes, et cetera. The price of fossil and energy storage and construction materials was significantly increased due to the COVID pandemic, the Russian-Ukrainian war, the global financial crisis, etc. Without optimization, the cost of logistics can be increased, which influences the result of a project's cost-benefit analysis (CBA) anywhere in the world.

Nowadays, the research dealing with railway infrastructure and connecting to ballast concentrate on many topics, e.g., non-exhausting, increasing the resistance against breakage [14, 15, 17], and considering point load test to classify them [18], etc.

The main lines' traffic is loaded with passenger and freight trains; however, the industrial sidings and mine tracks [19, 20] are utilized for transportation in the production process. Cur-

rent research is mainly related to standard public railways; however, the results can be applied to industrial sidings, mine tracks, tramways, and metros, as well. In addition, the authors have dealt with the determination of interlocking effect [21], GCCMs [22], as well as Digital Image Correlation (DIC) and GOM [23] in the past decade.

Statement of the problem. This article deals with railway lines that have lower maintenance costs. It is important to mention because the authors have experiences mainly in Hungary. On the other hand, if the research shows promising results, this solution could also solve other similar states or problems. So, the previously mentioned less-used railway lines also have serious problems, while the solutions can be cheap and ineffective. The primary solution is introducing a speed restriction that fits the track geometry maintenance limit values.

In this research, the authors look for solutions to prevent or maintain more significant substructural problems like weak substructure soil, water bags (water pockets), lack of drainage, etc. These problems can be fixed effectively by removing the whole superstructure, which is a time-consuming methodology. On the other hand, one intervention could increase the lifetime by many years. The question is, what is the most cost-effective solution? Is it worth spending much money on an underutilized railway line? Of course, the answer depends on the destination railway station's importance. If it is not worth it, the operator needs technologies or solutions which are cost-effective and easy to install without any external contractor.

One of these solutions is the geosynthetic cementitious composite mats (GCCMs), especially the Concrete Canvas (CC). These mats contain three layers. A fibrous fabric is on the top, while the lower layer is waterproof PVC (polyvinyl-chloride). These two are connected by a 3D fiber matrix, while a unique cement mixture fills it. According to official data scripts, the compressive strength reaches 80 % (but at least 50 MPa) after 24 hours of hydration. The notable types are CC5, CC8, CC13, and CCX. The numbers mean the thickness of the material in the 'mm' unit, while the CCX was made of Portland cement [22].

The hypothesis was that the CC deforms under loading, and the ballast particles are pressed (penetrated) into the CC. Thanks to this, the lower layers will be more stable, while the shear stress resistance will increase significantly. This state can be seen in Fig. 1. Furthermore, according to the function of the geogrid, the interlocking effect is created with this procedure.

The purpose of the article is to prove that the Concrete Canvas GCCM type can fulfill the same functions as geogrids and geomembranes. Thanks to the cemented material, the ballast's crushed stone particles can be pushed into the CC while it is bonded to the cement layer. Thanks to this, the shear stress resistance is increasing significantly.

Materials of the article. The investigations were performed in the laboratory of Széchenyi István University, Győr. In the 2010s, geogrids were investigated in this topic. Thanks to this, the multi-level shear box was given, and only the method and the layer structure were redesigned.

During the investigations, ballast crushed stone was andesite, with 31.5/50 mm grain sizes (i. e., the nominal minimum grain size was 31.5 mm; hence the maximum is 50 mm) according to the MSZ EN standard [24]. The sample was given by Colas Hungary Ltd., from the quarry of Szob, Hungary.

The authors planned to connect this research to other previous research from the 2010s, when geogrids and other geosynthetics were investigated for inner shear resistance. The related research was published in [21]. Thanks to this, the parameters had to be quite the same, i.e., E_2 load-bearing capacity [24] was tried to reach.

In the current article, the CC was purchased from Concrete Canvas Ltd. Based on previous investigations, it was observed that the properties and characteristics of the materials reached a 95–96 % state after seven days of hydration. It is crucial because the fully cemented properties can be reached after 28 days. However, in the multi-level shear box, with 28-day cycles, it would need at least four months; however, it could not be handled. Thanks to this, the authors decided to measure it in 7-day cycles, which means the CCs were near at 95–96 % state.

A 3D laser scanner (GOM ATOS) was utilized for the laboratory experiments. The measuring system is easy and simple to use; the measurements can be carried out relatively quickly. GOM creates accurate 3D point clouds. Because of the low-frequency blue light, ambient light effects interfering with the measurement can be easily eliminated during digitalization. The device is measuring with an accuracy of 0.01 mm [25]. In the current research, the GOM is necessary to measure the so-called flatness on the surface of the CC. On the other hand, the depressions (deformation due to the particle penetration into the CC layer) can also be measured very well.

Methods. The measurements were executed in a multi-level shear box in October 2022. First, the layer structure had to be determined. Compared to the previous investigations, the now-considered one was less thick. With the original layer structure, the E_2 load-bearing capacity on the plane of the sandy gravel was 7.2 MPa, so that was the purpose of reaching for an adequate comparison. The thickness of the sandy gravel was approximately ~13 cm, as well as the 40 cm XPS layer was exchanged to under ballast mats (UBMs). In the first case, some wooden plates were above the steel plate under the thick sandy gravel layer. The reason is that the necessary elasticity was created by rubber plates (i.e., UBMs). With one layer of UBM (and 18 cm sandy gravel), the achieved bearing capacity was 18.1 MPa. With this, the results were significantly higher than the previous measurements, so the elasticity had to be increased. Then, three layers of rubber mats were applied with 13 cm of sandy gravel. With that layer structure, 5.8 MPa load-bearing capacity was reached, which is an appropriate value in the comparison. Under the rubber mats, the floor (support) was a steel plate. It can be seen in Fig. 2.

Sample No. 0 was performed, where CC was not incorporated in the layer structure. It was necessary to check the shearing resistance without any strengthening. Against the mixing of the sandy gravel and the ballast particles, one layer of geotextile was used. The experiences were adequate so that the CC measurements could be executed.

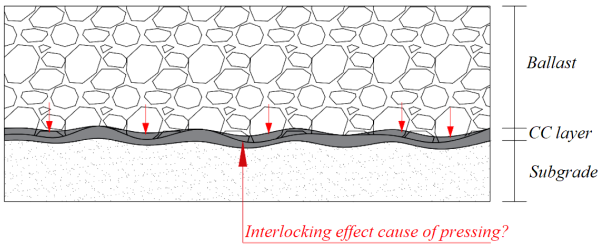

Fig. 1. Assumed behavior of the CC layer under the railway ballast

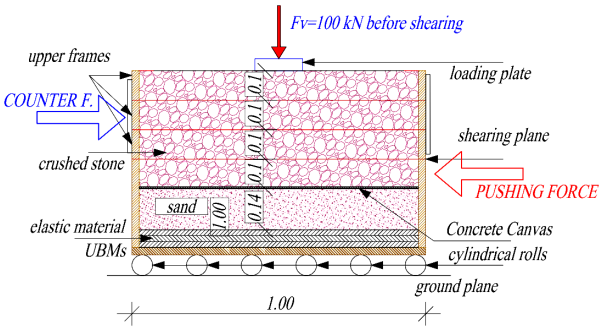

Fig. 2. The structure of the multi-level shear box

It is essential that before any investigation, the plane of the sandy gravel must be flat again, and it has to be recompacted. Because of this, these results can be more valid.

During the following measurements, the installation of the Concrete Canvas was critical. First, a 1.0 ×1.0 m sample was cut. It was essential to do it carefully, not to let the cement powder out. Then, before the hydration, it was surveyed by a 3D laser scanner, detailed in the previous paragraph (Fig. 3). It was crucial to know the flatness of the material at the beginning of the measurement.

For hydration, the material was watered carefully. The recommendation prescribes 9.5 liters per square meter until the material absorbs water. After the watering, 20 cm of crushed stone was laid and compacted. Next, a vibratory plate compactor was applied for the compaction. After the compaction, the layer structure was watered again. Then the next 20 cm was laid and compacted.

The authors aimed to reach the best possibility of this type of GCCM under the ballast, so it had to be loaded. It was decided that the well-compacted layer structure got a 100 kN load, which means nominal loading of 0.1 MPa (i.e., 10 N/cm^2). It was determined according to load distribution calculation/estimation [26].

After seven days of hydration under load, the sample was ready for laboratory experiments. According to creation of the interlocking effect, the inner shear resistance was measured 10 cm above the CC layer's plane because this parameter is assumed to be the largest at this level. During the measurement, the shear box had to be supported vertically. It was because the evolved torque wanted to rotate it – due to the contraction of the ballast –and the upper part of the box wanted to elevate (Fig. 4).

After the measurement processes, the ballast particles were removed from the box. The crushed stones were collected into three types of baskets. In the first basket, further usable stone particles were collected. The next phase was to collect the particles that were broken into small pieces or abrased and were smaller than 31.5 mm in diameter. The third collection was the particles pressed into the CC layer, and the CC cemented them under stress. These particles could not be removed by hand, only by a hammer. It is essential to mention that not all the particles were removed; some could not move without breaking. Therefore, these particles were also measured separately. In this case, the aim was to determine the lost material which stayed-remained in the CC.

After the ballast was entirely removed, the load-bearing capacity was measured on the surface. It was observed that the rigid CC did not break due to the 300 mm diameter plate loading. Therefore, it is due to the layer's load distribution.

The difference between the initial and final surface is significant; the material had a very irregular surface due to the ballast particles (Fig. 5). On the other hand, this state is spectacular and allows the contact surface to be checked under loading.

First, the contact surface can be measured graphically, showing how much the CC loaded. Second, the surface was again measured by a 3D laser scanner to show the resulting flatness.

After these steps, the measurement started from the beginning.

Results. First, it must be mentioned that the CC13 is relatively thin; it has only 1.3 cm thickness; on the other hand, it is rigid because of the hardened cement powder. This pair(ing) means that it is susceptible to breaking. It is not a significant problem because its structure enables good drainage in case of breakage, but in the case of railway loading, it could be a problem. At this measurement, the material did not break under loading; the sample came out ideally from the structure.

The evaluation of the measurement contained five phases:

1) measurement of inner shear resistance;
2) measurement of load-bearing capacity (E_2);
3) measurement of particle abrasion/breakage;
4) sign and evaluate the contact surface;
5) evaluation of the flatness of the CC from 3D laser scanner measurement helped by the GOM ATOS system.

The measured inner shear resistance can be seen in Table 1. However, the standard deviation is relatively high; the inner shear resistance increased significantly. The average of this parameter was 12 kN higher, which means a 52.04 % increase due to the CC. These values were compared to those of a similar investigation [21]. In this measurement, the shearing was only in one level (plane), i.e., 10 cm above the CC; however, in [21], the measurements were made in 4 levels (planes), 10–20–30 cm above the geogrids as well as in the lowest plane (i.e., the geogrids' plane). Current results were significantly higher than the values in [21], which can be due to the measurement process. The previous shear tests [21] were performed starting with shearing from the top plane, shifting the frame to the original position, and continuing the shearing of

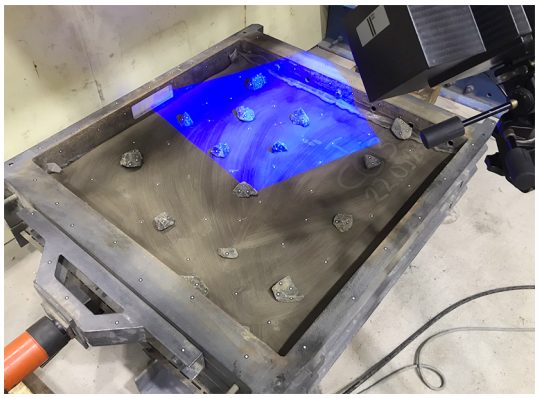

Fig. 3. 3D scanning of the CC sample by GOM ATOS

Fig. 4. The multi-level shear box during the shear test

Fig. 5. The surface of the CC after the shear test

Table 1

Results of the inner shear resistance (Sample No. 0 means the case Without CC; Samples Nos.1–3 are the cases Reinforced by CC)

Sample	Max. inner shear resistance, kN	Average, kN	Increasing, %	Standard deviation
No. 0	24.19	24.19	–	–
No. 1	32.62	36.78	52.04	4.295
No. 2	41.20			
No. 3	36.54			

the plane below it, until the lowest plane. However, current experiments were executed only in the plane 10 cm above the CC, so there was no disturbed layer and particles before the shearing, which can be the reason for the relatively high difference in the results.

The measurement graphs are shown in Fig. 6 and Table 2. In Fig. 6, the authors visualized the tangent of the inner shear resistance function with and without the Concrete Canvas in the 0–55 mm horizontal displacement interval. The changing of the inner shear resistance is relatively different related to the considered samples, but all of them significantly higher than the unreinforced case (Sample No. 0, Fig. 6). To be able to determine the tangent of the inner shear resistance graph, an interval was needed which is nearly the same at every case. For that, the 5–15 mm was determined. As it is seen, the average tangent is nearly 2.5 times larger than the unreinforced case (Table 2).

The other path is to compare the measurements by calculating the area under the graphs by integration, contained in Fig. 6. It was executed with different intervals than in Table 2. The graph of Sample No. 0 is even, so the chosen interval was the 0–40 mm section. It is also seen here that the standard

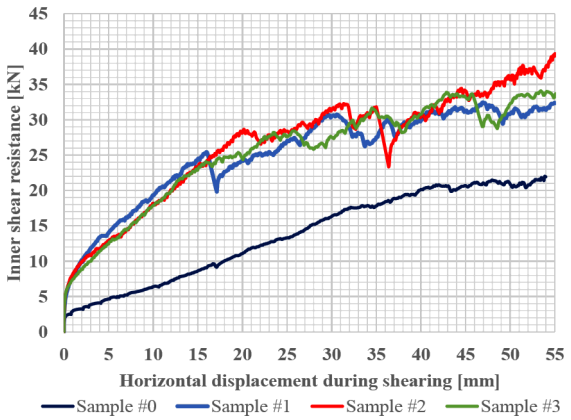

Fig. 6. Comparison of the inner shear resistance in a 0–55 mm horizontal displacement (shearing) interval

Table 2

The results of the tangent of the inner shear resistance in the 5–15 mm interval

Interval 5–15 mm			
Sample	Tangent	Ratio	Average ratio
No. 0	2.46	1.000	1.000
No. 1	1.04	2.386	2.470
No. 2	1.08	2.477	
No. 3	1.10	2.534	

deviation is relatively large, and the peak values are far from each other. Nevertheless, the results were an average of 3.18 times larger than the base measurement.

As mentioned earlier, the load-bearing capacity (E_2) was measured before and after the measurement. The base load-bearing capacity was only 5.8 MPa, but the average improved E_2 was 11.425 MPa, nearly two times better. So the improvement was not so considerable but unquestionable. The results of these tests are seen in Table 4.

The next part was the collection of the ballast particles. The abrasion (breakage) and the other results were calculated from the measurement of the weight of the whole ballast material. The weight of the cemented ballast particles and the abrasion were determined in the kg unit. They are shown in Tables 5 and 6. The cemented ballast particles were crucial in this measurement. First, the loads went through these crushed stone particles while pressed into the CC. Thanks to this state, the cemented ballast particles were unmovable and could close/compress the other stone particles. This effect is very similar to the effect of the geogrid (the so-called geogrid's interlocking effect). This significant result shows that the CC could stabilize the lower ballast well.

After the cemented ballast particles were removed, the particles let some kind of craters be seen very well in the photos. It is because when the particles were pressed into the CC layer, the special cement powder comes through the fibrous fabric (a kind of geotextile). Based on that, cementation surrounds the ballast particles, and after the stone particles are removed, the "crater" is formed. That is seen in Fig. 5, too.

It provides to measure the contact surface with a graphical evaluation. Thanks to this, the contact surfaces were signed with red color (Fig. 7), and then the area was calculated by CAD software. The calculated areas are shown in Table 7. It must be mentioned that the measurement in this way is not 100 % correct, but it shows us well the contact surface where the load distribution happens. According to this, the loading on the CC was not the nominal 10 N/cm^2 loading from [26]; it was 20.63 N/cm^2 instead.

According to the GOM ATOS system, the deformation of the CC's plane can be shown visually (Fig. 8), and a so-called flatness parameter can determine it. These values were collected in Table 8. The flatness value is used in mechanical engineering regulated by ISO 1101 [27]. During the evaluation,

Table 3

Calculating the area under graphs by integration in the 0–40 mm interval

Interval 0–40 mm			
Sample	Area, kN·mm	Ratio	Average
No. 0	505.76	1.000	1.000
No. 1	1446.10	2.860	3.180
No. 2	2127.26	4.210	
No. 3	1249.98	2.470	

Table 4

Results of the measuring of load-bearing capacities

Sample	E_2, MPa		Average	Standard deviation, MPa
	Before shearing	After shearing	MPa	
No. 0	5.8		–	–
No. 1	5.8	10.71	11.703	0.703
No. 2	5.8	12.22		
No. 3	5.8	12.18		

Table 5

The amount of the cement particles

Sample	Cement particles, kg	Average, kg	Standard deviation, kg	Weight perc., %	Avr. w.p., %
No. 1	37.21	39.643	2.565	6.41	6.853
No. 2	43.19			7.47	
No. 3	38.53			6.68	

Table 6

The amount of the broken particles

Sample	Abrasion/ breakage, kg	Average, kg	Standard deviation, kg	Weight perc., %	Avr. w.p., %
No.1	1.21	1.172	0.151	0.21	0.200
No.2	1.30			0.22	
No.3	1.01			0.17	

Table 7

Evaluation of the contact surface between the lowest layer of ballast and CC

Sample	Full area	Contact area	Ratio	Average	Standard dev.
	m^2	m^2	%	%	%
No. 1	1.01	0.49	48.51	48.48	0.854
No. 2	1.03	0.51	49.51		
No. 3	0.97	0.46	47.42		

Fig. 7. Evaluation of the contact surface on a 1×1 m large CC sample

the inner plane was measured because the sides of the material bent up. It could happen because the sample was bigger than the 1 × 1 m frame but it changed nothing in the results. Therefore, Fig. 8 is like the graphical evaluation of Fig. 7.

In Fig. 8, the amount of pressing can be seen by the 3D laser scanning. It was measured with an accuracy of 0.01 mm; another important thing is the evaluation of that. The device creates a baseline in the middle. According to it, the red color is above this level, while the blue is below. Theoretically, the load distribution was the same on the whole plane, but it can be seen that the middle area has more light blue colors, and the

Table 8

Evaluation of the 3D laser scanning according to [27]

Sample	Hydration, days	Flatness	Average	Stand. dev.
No. 0	0	12.68	–	–
No. 1	7	25.28	28.63	5.799
No. 2	7	25.29		
No. 3	7	35.33		

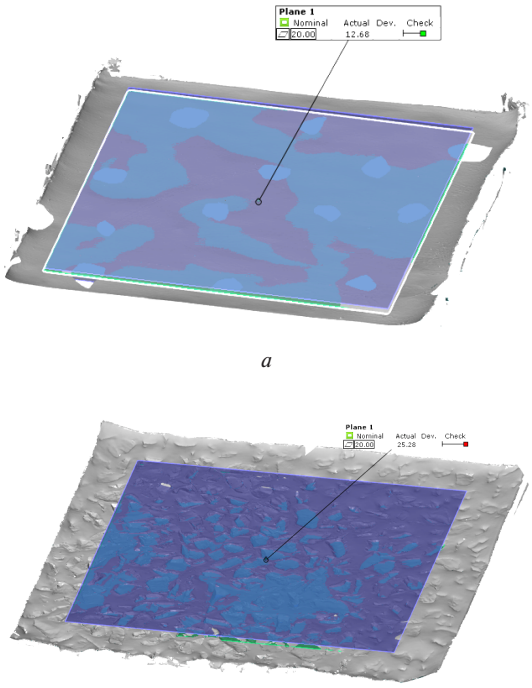

a

b

Fig. 8. Flatness evaluation of the 3D laser scanning: a – before the test; b – and after the test

outer area has more yellow, so most of the loading reached this inner zone. As the authors mentioned, the tested CC is 13 mm thick, so the 7–8 and more mm pressing (on an individually set baseline) were very large comparing the total thickness. The sign shows a particle, which was not able to remove. The procedure in Fig. 9 is more spectacular and accurate than in Fig. 7, while the substance is nearly identical.

Conclusions. This research was executed to prove that the Concrete Canvas (CC) can fulfill (or supplement) the geogrids and geomembranes functions. The drainage function was known

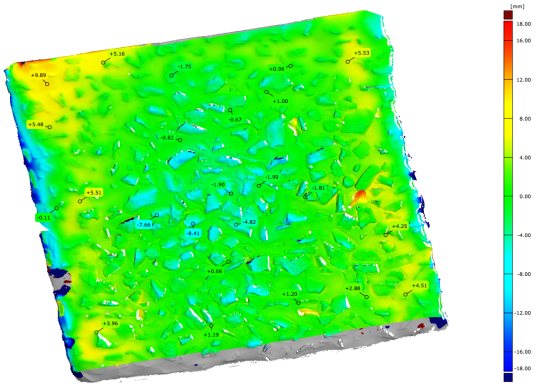

Fig. 9. Visual evaluation of the 3D laser scanning after the test

before, but the reinforcement function has not been investigated yet. From the multi-level shear box tests, the interlocking effect was proved. Furthermore, the inner shear resistance increased significantly due to the pressed and cemented ballast particles. These gave stabilization in the lower 10 cm zone.

Although, it must be mentioned that the laboratory experiments were performed assuming the so-called best condition. It means that the ballast above the CC received enough load(s) to press into the CC layer, more significant than the so-called normal load. Therefore, to compare the data to previous experiments with geogrids, the authors have to think about less loading before tests, and the shearing should be made on three levels instead of one.

To summarize the results, the Concrete Canvas provides adequate stabilization in the railway ballast.

References.

1. *European Commission, Mobility and Transport* (2022, November 30). Retrieved from https://transport.ec.europa.eu/transport-themes/infrastructure-and-investment_en.

2. Wang, L., Song, Y., Zhang, W., & Ling, X. (2023). Condition-based inspection, component reallocation and replacement optimization of two-component interchangeable series system. *Reliability Engineering & System Safety, 230*, 108907. https://doi.org/10.1016/j.ress.2022.108907.

3. Goodarzi, S., Kashani, H.F., Oke, J., & Ho, C.L. (2022). Data-driven methods to predict track degradation: A case study. *Construction and Building Materials, 344*, 128166. https://doi.org/10.1016/j.conbuildmat.2022.128166.

4. Kovalchuk, V.V., Sysyn, M.P., Hnativ, Y.M., Onyshchenko, A., Koval, M., Tiutkin, O.L., & Parneta, M. (2021). Restoration of the bearing capacity of damaged transport constructions made of corrugated metal structures. *Baltic Journal of Road and Bridge Engineering, 16*(2), 90-109. https://doi.org/10.7250/bjrbe.2021-16.529.

5. Sysyn, M., Gerber, U., Kluge, F., Nabochenko, O., & Kovalchuk, V. (2020). Turnout remaining useful life prognosis by means of on-board inertial measurements on operational trains. *International Journal of Rail Transportation, 8*(4), 347-369. https://doi.org/10.1080/23248378.2019.1685918.

6. Wang, X., Ding, Y., Zhao, J., Ji, L., Mao, C., & Zhuang, Y. (2023). Feasibility study on the solution of replacing track slab with lateral pushing rail in one maintenance window time. *Construction and Building Materials, 362*, 129658. https://doi.org/10.1016/j.conbuildmat.2022.129658.

7. Kurhan, M., Kurhan, D., & Hmelevska, N. (2022). Maintenance Reliability of Railway Curves Using Their Design Parameters. *Acta Polytechnica Hungarica, 19*(6), 115-127. https://doi.org/10.12700/APH.19.6.2022.6.9.

8. Kuchak, A.J.T., Marinkovic, D., & Zehn, M. (2020). Finite element model updating – Case study of a rail damper. *Structural Engineering and Mechanics, 73*(1), 27-35. https://doi.org/10.12989/sem.2020.73.1.027.

9. Kuchak, A.J.T., Marinkovic, D., & Zehn, M. (2021). Parametric Investigation of a Rail Damper Design Based on a Lab-Scaled Model. *Journal of Vibration Engineering and Technologies, 9*(1), 51-60. https://doi.org/10.1007/s42417-021-00341-7.

10. Macura, D., Laketić, M., Pamučar, D., & Marinković, D. (2022). Risk Analysis Model with Interval Type-2 Fuzzy FMEA – Case Study of Railway Infrastructure Projects in the Republic of Serbia. *Acta Polytechnica Hungarica, 19*(3), 103-118. https://doi.org/10.12700/APH.19.3.2022.3.9.

11. Naumov, V., Zhamanbayev, B., Agabekova, D., Zhanbirov, Z., & Taran, I. (2021). Fuzzy-logic approach to estimate the passengers preference when choosing a bus line within the public transport system. *Communications – Scientific Letters of the University of Žilina, 23*(3), A150-A157. https://doi.org/10.26552/com.C.2021.3.A150-A157.

12. Saukenova, I., Oliskevych, M., Taran, I., Toktamyssova, A., Aliakbarkyzy, D., & Pelo, R. (2022). Optimization of schedules for early garbage collection and disposal in the megapolis. *Eastern-European Journal of Enterprise Technologies, 1*(3-115), 13-23. https://doi.org/10.15587/1729-4061.2022.251082.

13. Milosevic, M., Pålsson, B., Nissen, A., Johansson, H., & Nielsen, J.C.O. (2023). Model-Based Remote Health Monitoring of Ballast Conditions in Railway Crossing Panels. *In: Rizzo, P., Milazzo, A. (eds) European Workshop on Structural Health Monitoring. EWSHM 2022. Lecture Notes in Civil Engineering, 253*. Springer, Cham. https://doi.org/10.1007/978-3-031-07254-3_51.

14. Czinder, B., Vásárhelyi, B., & Török, Á. (2021). Long-term abrasion of rocks assessed by micro-Deval tests and estimation of the abrasion process of rock types based on strength parameters. *Engineering Geology, 282*, 105996. https://doi.org/10.1016/j.enggeo.2021.105996.

15. Szabó, B., Pásthy, L., Orosz, Á., & Tamás, K. (2022). The Investigation of Additively Manufacturing and Moldable Materials to Produce Railway Ballast Grain Analogs. *Frattura ed Integrità Strutturale, 60*, 213-228. https://doi.org/10.3221/IGF-ESIS.60.15.

16. Rao, P.K.V., Varma, G.R.P., & Vivek, K.S. (2022). Structural dynamic analysis of freight railway wagon using finite element analysis. *Materials Today: Proceedings, 66*(3), 967-974. https://doi.org/10.1016/j.matpr.2022.04.770.

17. Sweta, K., & Hussaini, S.K.K. (2022). Role of particle breakage on damping, resiliency and service life of geogrid-reinforced ballasted tracks. *Transportation Geotechnics, 37*, 100828. https://doi.org/10.1016/j.trgeo.2022.100828.

18. Koohmishi, M. (2021). Assessment of strength of individual ballast aggregate by conducting point load test and establishment of classification method. International *Journal of Rock Mechanics and Mining Sciences, 141*, 104711. https://doi.org/10.1016/j.ijrmms.2021.104711.

19. Taran, I.A., & Klimenko, I.Yu. (2014). Transfer ratio of double-split transmissions in case of planetary gear input. *Naukovyi Visnyk Natsionalnoho Hirnychoho Universytetu,* (6), 60-66.

20. Samorodov, V., Bondarenko, A., Taran, I., & Klymenko, I. **(**2020). Power flows in a hydrostatic-mechanical transmission of a mining locomotive during the braking process. *Transport Problems, 15*(3), 17-28. https://doi.org/10.21307/TP-2020-030.

21. Fischer, S. (2017). Breakage test of railway ballast materials with new laboratory method. *Periodica Polytechnica Civil Engineering*, *61*(4), 794-802. https://doi.org/10.3311/PPci.8549.

22. Eller, B., Movahedi Rad, M., & Fischer, S. (2022). Laboratory Tests and FE Modeling of the Concrete Canvas, for Infrastructure Applications. *Acta Polytechnica Hungarica, 19*(3), 9-20. https://doi.org/10.12700/APH.19.3.2022.3.2.

23. Szalai, S., Eller, B., Juhász, E., Movahedi, M.R., Németh, A., Harrach, D., Baranyai, G., & Fischer, S. (2022). Investigation of deformations of ballasted railway track during collapse using the Digital Image Correlation Method (DICM). *Reports in Mechanical Engineering, 3*(1), 258-282. https://doi.org/10.31181/rme20016032022s.

24. Hungarian Standards Institute (2003). *MSZ EN 13450:2003. Aggregates for railway ballast*. Retrieved from https://ugyintezes.mszt.hu/webaruhaz/szabvanyadatok?standard=109857.

25. R-Design Studio (2022, November 30). *Metrology*. Retrieved from http://http://r-design.hu/.

26. Lichtberger, B. (2005). *Track compendium*. Eurailpress Tetzlaff-Hestra GmbH & Co. KG, Hamburg.

27. International Organization for Standardization (2017). *ISO 1101:2017. Geometrical product specifications (GPS) — Geometrical tolerancing — Tolerances of form, orientation, location and run-out*. Retrieved from https://www.iso.org/obp/ui#iso:std:iso:1101:ed-4:v1:en.

Ефект підвищення опору внутрішньому зсуву бетонного полотна баластного шару залізничної колії

В. Еллер[1,2], *С. Салаї*[1], *М. Сисин*[3], *Д. Гаррах*[1], *Я. Лю*[4], *Ш. Фішер*[*1]

1 – Університет Сечені Іштвана, м. Д'єр, Угорщина

2 – Печський університет, м. Печ, Угорщина

3 – Інститут залізничних систем і громадського транспорту, ТУ Дрезден, м. Дрезден, Федеративна Республіка Німеччина

4 – Південно-західний університет Цзяотун, м. Чэнду, Китайська Народна Республіка

* Автор-кореспондент e-mail: fischersz@sze.hu

Мета. Довести, що GCCM (геосинтетичний цементний композитний матеріал) – тип Concrete Canvas є адекватним додатковим прошарком баластного шару залізничної колії. Оскільки його дренажна функція відома, у цій роботі робиться спроба довести можливість армування. Цей прошарок відносно тонкий, проте його властивості подібні до георешіток. Це основний шлях до

з'ясування можливості ефекту блокування та його впливу на опір внутрішньому зсуву баластного шару залізничної колії.

Методика. Лабораторні виміри проводилися на устаткуванні «multi-level shear box», що дозволяє моделювати багаторівневий зсув баластного шару. Випробування було заплановано із прошарком Concrete Canvas і без нього. Після зсуву зразки були також випробувані на несучу здатність (E2; згідно з Угорським стандартом) і руйнування частинок. З іншого боку, поверхня контакту між нижньою частиною баласту та прошарком Concrete Canvas була виміряна за допомогою складного лазерного 3D сканера GOM ATOS і графічно за допомогою програмного забезпечення AutoCAD.

Результати. Після аналізу результатів проведених лабораторних експериментів розраховані й визначені наступні параметри: 1) коефіцієнт армування як тангенс кривих внутрішнього опору зсуву в інтервалі горизонтального зсуву 5–15 мм, а також площа під графіками інтегрування в інтервалі 0–40 мм; 2) зміна несучої здатності шаруватої структури з Concrete Canvas та без; 3) кількість цементованих частинок; 4) кількість зруйнованих частинок; 5) поверхня контакту між нижнім шаром баласту і Concrete Canvas; 6) площинність листів Concrete Canvas після зсуву. Згідно з отриманими результатами, бетонне полотно Concrete Canvas забезпечує значне посилення баластного шару залізничної колії.

Наукова новизна. Будь-який інший вид вимірювання бетонного полотна Concrete Canvas за допомогою устаткування «multi-level shear box» невідомий. Тема є унікальною.

Практична значимість. У майбутньому ці результати зможуть забезпечити вихідні дані для перевірки придатності залізобетонного полотна при його застосуванні у верхній і нижніх будовах рейкових колії для різних видів транспорту.

Ключові слова: *залізниця, зношення, бетонне полотно, баластний прошарок, внутрішній опір зсуву, блокувальний ефект, GOM ATOS*

The manuscript was submitted 05.12.22.